Available online at www.sciencedirect.com
ScienceDirect
International Journal of Mass Spectrometry 264 (2007) 38–52
International Journal of Mass Spectrometry
www.elsevier.com/locate/ijms

Geometry optimization of axially symmetric ion traps

Pavan K. Tallapragada [a], Atanu K. Mohanty [b], Anindya Chatterjee [c], A.G. Menon [a,*]

[a] *Department of Instrumentation, Indian Institute of Science, Bangalore 560012, India*
[b] *Supercomputer Education and Research Centre, Indian Institute of Science, Bangalore 560012, India*
[c] *Department of Mechanical Engineering, Indian Institute of Science, Bangalore 560012, India*

Received 12 January 2007; received in revised form 20 March 2007; accepted 20 March 2007
Available online 30 March 2007

Abstract

This paper presents numerical optimization of geometries of axially symmetric ion traps for mass analyzers. Four geometries have been taken up for investigation: one is the well known cylindrical ion trap (CIT) and three others are new geometries. Two of these newer geometries have a step in the region of the midplane of the cylindrical ring electrode (SRIT) and the third geometry has a step in its endcap electrodes (SEIT). The optimization has been carried out around different objective functions composed of the desired weights of higher order multipoles. The Nelder-Mead simplex method has been used to optimize trap geometries. The multipoles included in the computations are quadrupole, octopole, dodecapole, hexadecapole, ikosipole and tetraikosipole having weights A_2, A_4, A_6, A_8, A_{10} and A_{12}, respectively. Poincaré sections have been used to understand dynamics of ions in the traps investigated.

For the CIT, it has been shown that by changing the aspect ratio of the trap the harmful effects of negative dodecapole superposition can be eliminated, although this results in a large positive A_4/A_2 ratio. Improved performance of the optimized CIT is suggested by the ion dynamics as seen in Poincaré sections close to the stability boundary. With respect to the SRIT, two variants have been investigated. In the first geometry, A_4/A_2 and A_6/A_2 have been optimized and in the second A_4/A_2, A_6/A_2 and A_8/A_2 have been optimized; in both cases, these ratios have been kept close to their values reported for stretched hyperboloid geometry Paul traps. In doing this, however, it was seen that the weights of still higher order multipoles not included in the objective function, A_{10}/A_2 and A_{12}/A_2, are high; additionally, A_{10}/A_2 has a negative sign. In spite of this, for both these configurations, the Poincaré sections predict good performance. In the case of the SEIT, a geometry was obtained for which A_4/A_2 and A_6/A_2 are close to their values in the stretched geometry Paul trap and the higher even multipoles (A_8/A_2, A_{10}/A_2 and A_{12}/A_2) are all positive and small in magnitude. The Poincaré sections predict good performance for this configuration too. Finally, direct numerical simulations of coupled nonlinear axial/radial dynamics also predict good performance for the SEIT, which seems to be the most promising among the geometries studied here.

Keywords: Cylindrical ion trap; Nonlinear rf ion trap; Geometry optimization; Poincaré section

1. Introduction

This paper presents numerical optimization of geometries of axially symmetric rf ion traps for mass analyzers. The Nelder-Mead simplex method has been used to obtain geometry parameters for the mass analyzers by minimizing objective functions which incorporate desired weights of multipole superposition within the field. The motivation of this study is to show how standard, well known techniques can be used effectively in designing mass analyzers for high performance applications. Here, we have demonstrated the use of the technique to optimize the well known CIT of Wu et al. [1], and two variants of the CIT, of which one has a step on the ring electrode and the other has a step on its endcap electrodes. More generally, the technique can be used to design any axially symmetric mass analyzer.

The geometry of the cylindrical trap differs from that of the traditional Paul trap in that the hyperboloid electrodes of the latter trap are replaced by a cylindrical ring electrode and two planar end cap electrodes. This simplified geometry was first proposed by Langmuir et al. [2] for an ion storage device and subsequently used in mass spectrometry [3–5]. More recently, Cooks and coworkers have carried out extensive investigations on these mass

* Corresponding author. Tel.: +91 80 2293 2487; fax: +91 80 2360 0135.
E-mail addresses: pavant@isu.iisc.ernet.in (P.K. Tallapragada), anindya100@gmail.com (A. Chatterjee), amohanty@serc.iisc.ernet.in, agmenon@isu.iisc.ernet.in (A.G. Menon).

1387-3806/$ – see front matter © 2007 Elsevier B.V. All rights reserved.
doi:10.1016/j.ijms.2007.03.015

analyzers and have demonstrated their use in both mass selective boundary ejection and resonance ejection experiments [1,6–10]. The cylindrical ion trap proposed by them, however, has relatively poor resolution and this has limited its use to fieldable applications.

In the mass spectrometry literature, two approaches have been used to optimize geometries of mass analyzers. In the first, which is purely empirical and which is exemplified by the stretched geometry Paul trap, the serendipitous discovery that stretching improved mass calibration led to a systematic search to find the optimum geometry [11]. This resulted in the now well known 10.8% stretch associated with some Paul traps which are commercially available. In the second approach, adopted by Cooks and co-workers [1], numerical computations of field composition were first carried out on candidate geometries and, after manually identifying a few geometries (using the rough "−10% compensation" rule), the multi-particle simulation program ITSIM [12] was used to simulate mass spectra and empirical verification was carried out to identify the best of those geometries.

For hyperboloid geometry mass analyzers it is well known that trap performance is largely determined by its multipole field composition. In mass selective boundary ejection experiments, early numerical simulations of Franzen and co-workers [13–16] showed that positive even multipole fields cause early ejection of ions and negative even multipoles and odd multipoles of either sign result in delayed ejection. The analytical study of Sudakov [17] went further to show that early and delayed ejection occurs on account of the nature of the potential well associated with positive octopole, on the one hand, and negative octopole and hexapole of either sign, on the other.[1] In the former case, a single effective potential well exists and the depth and width of this well decreases as the operating point of an ion approaches the stability boundary. In the latter case, the existence of a double well in the unstable region of the Mathieu plot caused delayed ejection. In resonance ejection experiments [18] too, field inhomogeneities have been known to effect trap performance [19]. Makarov [20] and Rajanbabu et al. [21] have investigated and elaborated on the role of positive octopole superposition in enhancing mass resolution.

In a recent analytical study reported in Rajanbabu et al. [22] which incorporates multipoles up to dodecapole, a more detailed insight has been obtained on the role of field inhomogeneities on trap performance. The phase portraits obtained from the slow flow for positive even multipoles show one stable fixed point at the origin, and two outlying saddles. For slow enough scan rates, all ions of a given mass are confined within the stable region close to the origin. As the operating point approaches the stability boundary, the area of the stable region shrinks and the outlying saddles approach each other until, at an operating point close to the stability boundary, the stable fixed point is annihilated and ejection of many ions occurs simultaneously. This results in good resolution observed in mass spectra. In the case of negative even multipoles and odd multipoles of either sign, even beyond the nominal stability boundary the phase portraits display two stable equilibria away from the origin. The origin is now an unstable saddle. In traps with these inhomogeneities, ion detection occurs only when its oscillation amplitude increases beyond the trap boundary; this does not happen simultaneously for all ions of a given mass, and poor resolution is obtained.

Although the numerical and analytical studies above were carried out to understand contributions of specific multipoles, we can extend them to situations where there are combinations of multipoles. Based on simulations reported in Rajanbabu et al. [22], we conclude that good performance can be expected when the nonlinear trap has predominantly weak higher order positive even multipoles and poorer performance can be expected in traps having negative even multipoles and/or odd multipoles of either sign. In the context of Poincaré sections this would imply that good performance will be predicted by a single stable fixed point at the origin and relatively poor performance by multiple stable fixed points.

Before we present the scope of the paper, we list a few general ideas that we consider important in the context of optimizing trap geometries.

1.1. Standpoint of this paper

First, weak nonlinearities in the trapping field can have a significant effect on resolution. In particular, weak nonlinearities of the right kind can significantly enhance resolution. This conclusion follows from ample mathematical investigations to be found in Refs. [13–17] and our own earlier work [21–23]. We emphasize that the study of nonlinear fields in Paul traps was initially motivated by attempts to understand the effect of non-ideal geometries (e.g., holes and truncation); but the conclusion of theoretical studies that certain nonlinearities can be helpful is independent of the original motivation (non-ideal geometries).

Second, during normal trap operation, at the end of the cooling period, ions are expected to be somewhere close to the center of the trap, i.e., their oscillation amplitudes are somewhat small compared to the trap dimension. Subsequently, as the resonance or boundary ejection point is approached, the ion motion grows predominantly in the axial direction. Since we assume small initial amplitudes and subsequent growth in predominantly axial motions, we will study the dynamics of axial motions only. Such axial motions can be fruitfully (and rigorously) studied using Poincaré sections, which will be our primary evaluation tool for the optimized geometries we calculate.

Third, having focussed on axial motions alone, we must admit the possibility of significant radial direction dynamics. We will study this issue after the fact, using nonlinear simulation of the axial/radial coupled field equations.

Fourth, any significant departure from the perfect hyperboloid geometry, such as use of closed cavity shapes like cylinders, or the introduction of holes, is likely to produce strong nonlinearities close to the trap boundary. For example, near corners and holes, it is not expected that the low-order and weak nonlinearities we use in our study will do a good job of describing the ion dynamics. Additionally, close to the endcap holes, the

[1] Weights of multipoles are expressed as ratios of the strengths of these multipoles to the strength of the quadrupole.

ion feels the spatially localized effect of the ion detector. How the ion detector pulls the ion towards itself is, therefore, a matter of engineering that lies outside usual theoretical analyses of ion dynamics in the trap. To see that higher order nonlinearities are relatively unimportant except close to the endcaps, consider the discussion in Plass et al. [24] where they say a nonlinear term of order z^{22} represents the contribution of holes. Assume that we are interested, at ejection, in some $z = z_0$ (say, the axial dimension of the trap). When the ion amplitude is smaller, say $z = 0.75z_0$, then the same term in comparison with the linear term is 0.75^{21}, i.e., more than 400 times smaller. In this way, very high order nonlinearities are typically important only where our analysis stops and the ion detector takes over.

Fifth, we emphasize that all results in this paper are based on theory and simulation; and these in turn are based on simplifying assumptions as delineated above. Therefore, the *final* evaluation of the trap geometries found in this paper must be through experiment. The emphasis of this paper, however, remains on development and description of a methodology for systematically optimizing candidate trap geometries which might then be experimentally probed with greater expectations of success.

Finally, we note that our general optimization goals might be met by many candidate objective functions. In this we agree with, e.g., Klahr's comment from 1958 [25]:

> "One of the most difficult aspects of this problem ... is the choice of an objective function. The difficulty exists not because it is hard to find an objective function but rather because it is too easy."

It is not possible here to select any one objective function as the best; we will therefore consider a few such functions.

1.2. Scope of the paper

In this paper, we present numerical optimization of geometries of axially symmetric ion trap mass analyzers. We illustrate the scheme through the optimization of four traps. The first of these is a cylindrical ion trap (CIT0) reported by Wu et al. [1]; the other three are modified-CIT mass analyzers, of which two have a stepped-cylinder ring electrode while the third has a step (protrusion) in the endcap electrodes.

All our geometries have top-bottom symmetry, whereby all odd-order multipoles vanish. In line with the previous subsection, we will optimize these geometries using objective functions that, roughly speaking, aim for small and positive values for the even order multipole superpositions (as these are known to be beneficial). We consider objective functions which range from trying to match the known multipole strengths of the familiar stretched-hyperboloid geometry trap, to others where we seek small positive values by (a) penalizing all nonzero values and (b) penalizing negative values more strongly than positive ones.

Starting from the CIT0 of Wu et al. [1], we obtain, for purely cylindrical geometries, results that are not fully satisfactory. On the one hand, Wu et al.'s published geometry has a negative dodecapole superposition, which we believe compromises performance. On the other hand, the pure cylindrical geometry is sufficiently constrained (there is only one free parameter, namely the aspect ratio of the cylinder) that removal of the negative dodecapole leads to a somewhat large positive octopole. We report our results below for completeness, but move on to stepped cylinder geometries where better results are obtained. In particular, we introduce a stepped ring electrode ion trap (SRIT) and a stepped endcap electrodes ion trap (SEIT).

In this paper, we have included quadrupole, octopole, dodecapole, hexadecapole, ikosipole and tetraikosipole superpositions having weights A_2, A_4, A_6, A_8, A_{10} and A_{12}, respectively. The evaluation of trap geometries has been carried out through Poincaré sections generated near the nominal stability boundary ($q_z = 0.908$), which provides an insight into trap performance in mass selective boundary ejection experiments. Subsequent numerical simulations of coupled axial and radial motions have also been conducted.

The rest of the paper is organized as follows. In Section 2, we describe the methods that have been used to find the charge distribution and multipole coefficients, and to optimize the geometry. Also described in this section is the resulting equation of axial ion motion and the method to generate Poincaré sections. Section 3 presents the verification of the computations by comparing our results with those reported in the mass spectrometry literature. Section 4 discusses the results of our investigations. Section 5 presents some concluding remarks.

2. Field calculation and optimization

To compute charge distribution on the electrodes and the potential inside the ion trap for a given geometry, we have developed a MATLAB library which uses the boundary element method (BEM). This library can be used to define various axially symmetric geometries and also to specify the potential on different electrodes. The potential at a given point inside the trap is found by using the charge distribution on the electrodes. Using this, the multipole expansion coefficients, A_n, are calculated directly and, finally a chosen objective function which incorporates the desired multipole coefficients is minimized to obtain the optimized geometry of the trap. In the present study we include quadrupole, octopole, dodecapole, hexadecapole, ikosipole and tetraikosipole superpositions corresponding to multipole coefficients A_2, A_4, A_6, A_8, A_{10} and A_{12}, respectively. No odd multipoles occur in the present computations since we have assumed top-bottom symmetry in our geometries.

2.1. Charge distribution

In order to compute the charge distribution along the surface of the electrodes, the electrodes are computationally divided into N elementary rings. Fig. 1 shows two such rings on an arbitrary electrode. The ith ring is of width Δw_i, has a mean radius r_i and is at a mean axial distance z_i from the origin (the center of the trap), with a charge q_i assumed to be uniformly distributed on it. For small ring widths, Δw_i, the potential computed at distances large compared to Δw_i from the electrode will be a good approximation to the true potential, with an error in the potential proportional to Δw_i^2.

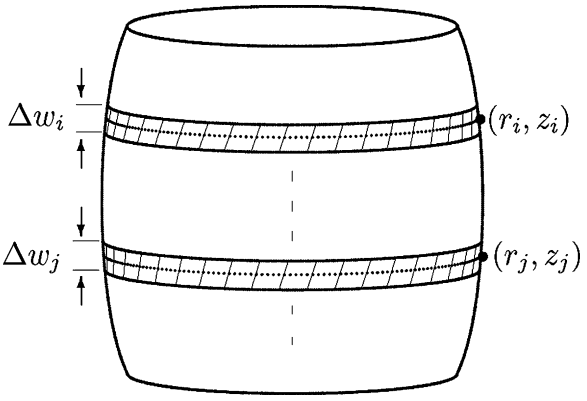

Fig. 1. Diagram of an arbitrary electrode and two arbitrary elementary rings.

For purposes of computation of the potential at points not on the ring, the charge is assumed to be concentrated on the circumference of mean radius r_i and at mean height z_i. Hence, for $i \neq j$ the potential at a point on the jth ring due to the ith ring is given by [26]

$$u_{i,j} = \frac{q_i}{4\pi\epsilon_0} \frac{2}{\pi\sqrt{(z_i - z_j)^2 + (r_i + r_j)^2}} K(k) = g(i, j)\, q_i \qquad (1)$$

where

$$K(k) = \int_0^{\pi/2} \frac{\mathrm{d}\beta}{\sqrt{1 - k^2 \sin^2 \beta}} \quad \text{and}$$

$$k^2 = \frac{4 r_i r_j}{(z_i - z_j)^2 + (r_i + r_j)^2},$$

and where ϵ_0 is the permittivity of free space. $K(k)$ is a complete elliptic integral of the first kind [27]. Because of axial symmetry, polar angle Φ does not appear in Eq. (1).

When $i = j$, the width of the elementary ring cannot be ignored (since ignoring the width would lead to a singularity) and the potential, $u_{i,i}$ can be derived to be

$$u_{i,i} = \frac{q_i}{4\pi\epsilon_0} \frac{1}{\pi r_i} \left(1 + \ln\left(\frac{16 r_i}{\Delta w_i}\right)\right) = g(i, i)\, q_i. \qquad (2)$$

The potential on the jth elementary ring is given by

$$u_j = \sum_{i=1}^{N} g(i, j)\, q_i \quad j = 1 \text{ to } N. \qquad (3)$$

Since the potentials u_j on the different electrodes are known a priori, the N linear equations in Eq. (3) can be solved simultaneously to get the charges, q_i $(i = 1 \ldots N)$, on the elementary rings. This charge distribution is used to compute the multipole coefficients of the field within the trap cavity.

2.2. Multipole coefficients

The potential at a point $u(\rho, \theta, \phi)$ in spherical coordinates, in an axially symmetric trap, can be expressed in terms of Legendre polynomials P_n. When a potential Φ is applied to the central electrode with endcaps kept at ground potential, $u(\rho, \theta, \phi)$ is given by [28]

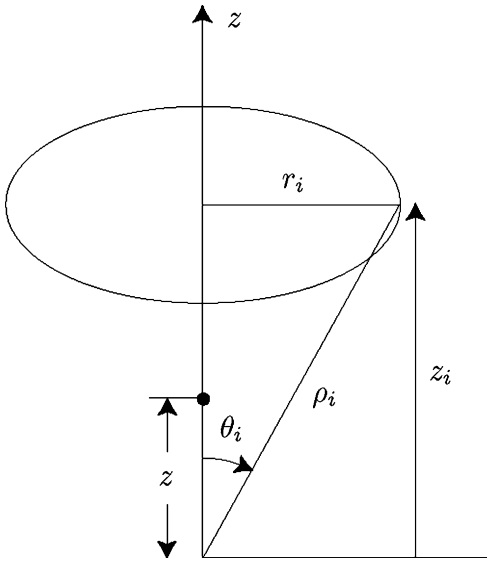

Fig. 2. Potential due to a ring at a point on its axis.

$$u(\rho, \theta, \phi) = \Phi \sum_{n=0}^{\infty} A_n \left(\frac{\rho}{L_N}\right)^n P_n(\cos\theta) \qquad (4)$$

where A_n are the coefficients that are to be found and L_N is a normalizing length.

To find A_n, we note that the potential at a point on the z-axis due to a ring as shown in Fig. 2 is given by [26],

$$u_i(z) = \frac{q_i}{4\pi\epsilon_0 \rho_i} \sum_{n=0}^{\infty} \left(\frac{z}{\rho_i}\right)^n P_n(\cos\theta_i) \qquad (5)$$

where q_i is the charge on the ring, z_i is the axial position of the ring, $\theta_i = \arctan(r_i/z_i)$ and $\rho_i = \sqrt{r_i^2 + z_i^2}$, r_i being the radius of the ring.

Since the electrodes have been divided into N rings, the potential at a point on the z-axis in the trap can be found by adding the potential due to each of the N rings and is seen to be

$$u(z) = \sum_{i=1}^{N} \frac{q_i}{4\pi\epsilon_0 \rho_i} \sum_{n=0}^{\infty} \left(\frac{z}{\rho_i}\right)^n P_n(\cos\theta_i). \qquad (6)$$

The potential $u(z)$ at a point on the z-axis can also be obtained from Eq. (4) setting $\rho = z$ and $\theta = 0$, and is given by

$$u(z) = \Phi \sum_{n=0}^{\infty} A_n \left(\frac{z}{R_N}\right)^n. \qquad (7)$$

By comparing the coefficients of z^n in Eqs. (6) and (7) we obtain

$$A_n = \frac{1}{\Phi} \sum_{i=1}^{N} \frac{q_i}{4\pi\epsilon_0 \rho_i} \left(\frac{L_N}{\rho_i}\right)^n P_n(\cos\theta_i). \qquad (8)$$

Note that q_i is proportional to the applied potential Φ and with Φ appearing in the denominator also, A_n maybe calculated with Φ set to 1.

In the mass spectrometry literature, the multipole coefficients are generally computed by a least squares fit [1,29] to the potential at a number of points in the trap. In contrast, our method, which is similar to that used by Beaty [28], computes the coefficients directly from the charge distribution.

2.3. Optimization

We have used the Nelder-Mead simplex method [30,31] for optimization of the trap geometry. This is a direct search method for finding the local minimum of a function of several variables. In this method, the function is evaluated at the vertices of a simplex (a triangle in 2D, a tetrahedron in 3D and so on). From an initial guess of the optimal point, the method iteratively shrinks the simplex to approach a possibly local minimum of the objective function. For a given objective function, the point to which the simplex converges to depends on the initial guess and the distance between the vertices of the simplex formed from it. In this work, the objective function is specified in terms of desired multipole coefficients as discussed later.

2.4. Poincaré sections

As exemplified by Cooks and co-workers, the final test for a trap lies in fabrication and experiment. However, in this theoretical work, we have optimized trap geometries for criteria involving multipole weights. Whether these specific values of multipole weights do in fact give good ion dynamics is investigated here, pending final experimental verification, through simulations of ion dynamics and Poincaré sections.

The equation of axial motion of an ion in a trap with no damping is

$$\frac{\mathrm{d}^2\bar{z}}{\mathrm{d}\tau^2} + (a_z + 2q_z\cos 2\tau)\sum_{n=2}^{\infty}\frac{A_n}{A_2}\frac{n}{2}\bar{z}^{n-1} = 0, \tag{9}$$

where $\bar{z} = z/L_N$ is the normalized axial position of the ion, $\tau = \Omega t/2$, Ω the angular frequency of the applied rf potential; and a_z and q_z are given by

$$a_z = \frac{8qA_2U}{mL_N^2\Omega^2}, \qquad q_z = \frac{4qA_2V}{mL_N^2\Omega^2}, \tag{10}$$

where q/m is the charge to mass ratio of the ion, U the applied dc potential and V is the zero-to-peak amplitude of the applied rf potential. Eq. (9) is a nonlinear Mathieu equation, and a_z and q_z are referred to as Mathieu parameters. In mass selective boundary ejection experiments the dc potential, U, is usually set to zero and hence a_z is 0.

In our study, all odd multipole coefficients are zero because of assumed top-bottom symmetry. Truncating the sum in Eq. (9) at $n = 12$ and setting $a_z = 0$, we have the following equation of motion

$$\frac{\mathrm{d}^2\bar{z}}{\mathrm{d}\tau^2} + 2q_z\cos 2\tau\sum_{n=2}^{12}\frac{A_n}{A_2}\frac{n}{2}\bar{z}^{n-1} = 0, \quad (n \text{ even}). \tag{11}$$

Eq. (11) is solved numerically using MATLAB to generate the Poincaré sections. For each of a number of initial conditions for $\bar{z}$ and $\mathrm{d}\bar{z}/\mathrm{d}\tau$ the evolution of the motion of the ion is strobed at the period of the parametric forcing (π units of scaled time τ) with an initial rf phase of π radians. A plot of $\bar{z}$ versus $\mathrm{d}\bar{z}/\mathrm{d}\tau$ is the Poincaré section for the specified weights of even multipole superpositions.

3. Verification

To verify our methods of field calculation and optimization, we have compared our results with data available in the literature. Three test geometries have been considered, the cylindrical ion traps as proposed by Kornienko et al. [32] and by Wu et al. [1] have been used to verify our field computations, and the stretched geometry Paul trap discussed by Franzen et al. [33] has been used to check our optimization. It will be shown that the methods adopted by us provide results that compare favourably with analytical and numerical results reported in the mass spectrometry literature.

3.1. Cylindrical ion trap of Kornienko et al.

We first look at cylindrical ion traps with no spacing between the ring electrode and the endcap electrodes, and with no holes in the endcaps. Kornienko et al. [32] give analytical expressions for multipole coefficients for such geometries. Table 1 presents a comparison of the multipole coefficients obtained analytically with those computed using BEM for two geometries.

It is seen that the numerically obtained coefficients match to three or more decimal places, which is acceptable for our purposes.

Table 1
Comparison of coefficients computed using BEM with those obtained from analytical expression reported in Ref. [32]

	Analytical [32]	BEM
$r_0 = 1,\ z_0 = 0.9$		
A_0	0.651037	0.651084
A_2	−0.848386	−0.848738
A_4	−0.072415	−0.072456
A_6	0.182100	0.182292
A_8	−0.003054	−0.003084
$r_0 = 1,\ z_0 = 1$		
A_0	0.721326	0.721390
A_2	−0.710093	−0.710364
A_4	−0.131167	−0.131260
A_6	0.120239	0.120359
A_8	0.023128	0.023159

Table 2
Comparison of coefficients found using BEM with those reported by Wu et al. [1] for cylindrical ion traps

CIT	Wu et al. [1]			BEM		
	A_2	A_4	A_6	A_2	A_4	A_6
CIT0	0.736	0.055	−0.131	−0.736	−0.054	0.133
CIT1	0.714	0.027	−0.162	−0.719	−0.033	0.156
CIT2	0.646	0.068	−0.130	−0.650	−0.072	0.127
CIT3	0.622	0.050	−0.117	−0.625	−0.054	0.115
CIT4	0.692	0.086	−0.157	−0.697	−0.093	0.151

Table 3
Comparison of coefficients for a Paul trap with a stretching of 10.8% as reported in Ref. [33] with those computed using BEM for a stretching of 9.68%

	Franzen et al. [33]	BEM
A_2	−0.894034	−0.907028
A_4	−0.014390	−0.014387
A_6	−0.006280	−0.006611
A_8	−0.000830	−0.002280
A_{10}	−0.000304	−0.001256
A_{12}	−0.000034	−0.000737

3.2. Cylindrical ion trap of Wu et al.

We next consider cylindrical ion traps with spacing between the ring electrode and the endcaps, with holes in the endcaps and with the electrodes having some thickness. Table 2 compares the coefficients for five different configurations of the cylindrical trap reported by Wu et al. [1] with those found by our method. Agreement here is to two decimal places. Note, however, that Wu et al. present numerical (as opposed to analytical) results, and so not all the variation observed need be from our method of computing coefficients of multipole expansion. In any case, agreement seems sufficient for practical purposes.

The inversion in sign of the coefficients under BEM in Table 2 is on account of the multipole expansion used by Wu et al. [1] being opposite in sign to that used by us. The convention that we have adopted is consistent with [28] and with the results reported in Table 1.

3.3. Geometry optimization

To verify our optimization technique as a whole, we have applied it to optimize the stretching of the endcaps from their ideal position in a truncated Paul trap. The objective function for the optimization has been chosen to force the coefficients of the multipole expansion to their reported values for the stretched hyperboloid geometry mass analyzer. The value of A_4 is reported to be −0.01439 [33] for a Paul trap with a stretching of 10.8% (the optimum stretching found empirically) and it is also known that A_2 in these stretched traps is close to unity. In view of this, an objective function F has been chosen involving only A_4 and A_2 and has the form

$$F = \left| \frac{A_4 + p}{A_2} \right|, \quad p = 0.01439.$$

Inclusion of A_2 in the denominator ensures that we focus only on those geometries in which A_2 is not small. At the minimum of the objective function, we can expect A_4 to have a value of $-p$, that is −0.01439.

In our computations, the radius of the ring electrode was taken as 7.1 mm and the truncation factor approximately[2] as 3. Our optimization was carried out with an initial guess for stretching as 0 (the ideal geometry). The stretching recommended by our computations was 9.68%, a number remarkably close to the empirically optimized stretch of 10.8% [11]. The difference (between 9.68% and 10.8%) is not on account of our optimization but due to several other factors. First, the objective function we have chosen includes only A_2 and A_4. Choice of a different objective function might lead to a closer match. Second, the difference in the truncation of the two traps would also lead to a mismatch in the stretch predicted by our optimization. Finally, mismatch could also arise because the value of p used by us in the objective function F has been taken from [33] where it was computed numerically.

The multipole weights obtained for our 9.68% stretch is compared with the those of the 10.8% stretch geometry reported in Ref. [33] in Table 3 and here too the general trend in the two columns appears to be similar. The marginal difference seen in the two columns is on account of the different degrees of stretch (10.8% and 9.68%) in the two geometries.

It is evident from the preceding paragraphs that the methods we have chosen for field computations and optimization provide results comparable to those reported in the mass spectrometry literature. We will next apply these methods to optimize the CIT, the SRIT and the SEIT. Our motivation for doing this is two fold. First, we wish to demonstrate how the automated scheme can be applied to achieve geometry parameters of cylindrical ion traps for a desired field configuration. Starting with a simple objective function for the CIT, we systematically impose greater constraints on the field configuration by modifying the objective function as we optimize the SRIT and the SEIT geometries. Second, through the geometries we investigate, we hope to present practically achievable geometries for mass spectroscopists to use. Here the underlying thought has been to keep the design simple for ease of fabrication (with the possibility of miniaturization) and still ensure that the performance of these analyzers is similar to the stretched geometry Paul traps.

4. Results and discussion

Before we proceed with our optimization, we digress briefly to highlight an important point that needs to be considered when comparing the coefficients of two traps with significantly different geometries. The potential at a point in the ion trap is expressed by a multipole expansion as in Eq. (4) and the coefficients of multipole expansion are computed by Eq. (8). In these equations, L_N is the normalization distance and, because this choice is arbitrary, a degree of caution needs to be exercised

[2] The computations were carried out using the exact dimensions of a trap in use in our laboratory.

Table 4
Comparison of the coefficients of multipole expansion of stretched geometry Paul trap, the CIT0, the CITopt, the SRIT1, the SRIT2 and the SEIT. The normalizing distance L_N for these coefficients is half the distance between the endcap electrodes, z_0

	Renormalized stretched Paul trap	CIT0	CITopt	SRIT1	SRIT2	SEIT
A_2	−0.548787	−0.736104	−0.570982	−0.885158	−0.860598	−0.526485
A_4	−0.005422	−0.054441	−0.548845	−0.008748	−0.008491	−0.005151
A_6	−0.001452	0.133471	−0.001513	−0.002374	−0.002140	−0.001249
A_8	−0.000118	−0.020861	0.241221	−0.071361	−0.000239	−0.026487
A_{10}	−0.000026	−0.019374	0.083049	1.012510	0.481817	−0.008819
A_{12}	−0.000002	0.016450	−0.099031	−3.347869	−1.478473	−0.000269
A_4/A_2	0.009880	0.073958	0.961229	0.009883	0.009867	0.009784
A_6/A_2	0.002647	−0.181320	0.002650	0.002681	0.002486	−0.002372
A_8/A_2	0.000215	0.028339	−0.422467	0.080619	0.000278	0.050310
A_{10}/A_2	0.000048	0.026319	−0.145450	−1.143874	−0.559863	0.016750
A_{12}/A_2	0.000003	−0.022347	0.173440	3.782225	1.717959	0.000512

when adopting the coefficients of one geometry for another. In the present study, we have chosen z_0, half the distance between the endcap electrodes, as the normalizing distance for all trap geometries. This choice may be understood by the fact that in axially symmetric mass analyzers, under study in this paper, the motion of the ions along the z-axis is the motion of interest. Hence, using z_0 of the respective analyzers as the normalizing distance for the computation of the multipole coefficients, a justifiable comparison of the coefficients and the ion dynamics can be made across different analyzers. In view of this, the coefficients for the stretched geometry Paul trap reported by Franzen et al. [33], shown in Table 3, will have to be renormalized with respect to z_0 for the purpose of their adaptation in cylindrical traps that we have investigated. When this is done, L_N, which in the original formulation was r_0 (r_0 being the radius of the ring electrode), is now replaced by $(1 + 0.108)(1/\sqrt{2})r_0$ which corresponds to z_0 of the 10.8% stretched trap. These renormalized coefficients are presented in Table 4. Also presented in this table are the coefficients for the CIT0 of Wu et al. [1] and for the different cylindrical trap geometries that we have optimized in the present study. All these coefficients are presented in the same table for easy comparison.

We next turn to study the dynamics of ions in a stretched geometry Paul trap through Poincaré sections. This will guide us in evaluating the performance of cylindrical traps that are being investigated. The Poincaré sections in Fig. 3 have been obtained from the strobed solutions to the equation of motion given by Eq. (11) for the stretched trap. Multipole coefficients up to A_{12} (which are shown in Table 4) have been used for the computations. The plots in Fig. 3 are for $q_z = 0.907$ and $q_z = 0.9079$, that is when the ions are within the stable region of the Mathieu plot but close to the stability boundary. The Poincaré sections reveal a stable center close to the origin and two saddle nodes on either side. As the ions approach the stability boundary (i.e., when its q_z value increases), the area of the stable central region shrinks. All ions of a given mass to charge ratio are ejected simultaneously when the stable center is annihilated. Such a behaviour has been shown to be associated with good resolution in the study reported in Ref. [22]. Consequently, our effort in optimizing the cylindrical traps will be to obtain ion dynamics which display similar behaviour.

We now return to the optimization of the CIT and three new stepped geometries. Due to the difference in the shapes of CIT, the stretched geometry trap and stepped geometry traps, the values of A_2 and other multipole expansion coefficients cannot be expected to be the same in these traps. We will instead use *ratios* of the coefficients of higher order multipoles to that of the quadrupole component (A_2) in our present work. Usage of ratios rather than the values of the multipole coefficients is in conformity with common convention in discussions related to contribution of higher order multipoles to ion dynamics (e.g., [17,22,20]).

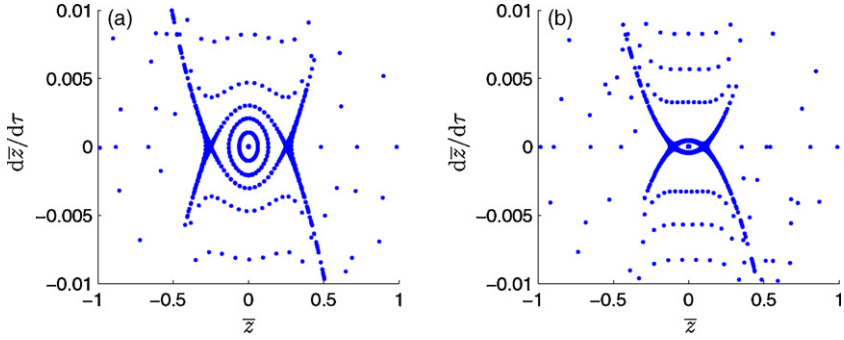

Fig. 3. Poincaré sections for stretched geometry Paul trap for q_z equal to (a) 0.907 and (b) 0.9079.

4.1. CIT optimization

The geometry parameters of CIT of Wu et al. [1] has been reproduced here in Fig. 4 for easy reference. In the figure the radius of the trap is r_0, the distance between the endcap electrodes is $2z_0$, the radius of the holes in the endcaps is r_H, length of the cylinder is z_b, the gap between the ring and the endcap electrodes is d_s, thickness of the ring electrode is r_b and the thickness of the endcap electrodes is d_E. These notations are identical to those used by Wu et al.

The dynamics associated with the CIT0 [1] can be seen in the Poincaré sections which have been obtained using the multipole coefficients reported in Table 4 for the CIT0.

The plots in Fig. 5a–e present the Poincaré plots for q_z values 0.898, 0.9, 0.906, 0.908 and 0.912, respectively. It can be seen that for $q_z = 0.898$, there is only one stable center, at the origin. At $q_z = 0.9$, we see a stable center at the origin, two saddle nodes on either side and two more stable centers further away. For higher values of q_z we see that the central stable region shrinks just as in the case of the stretched geometry Paul trap

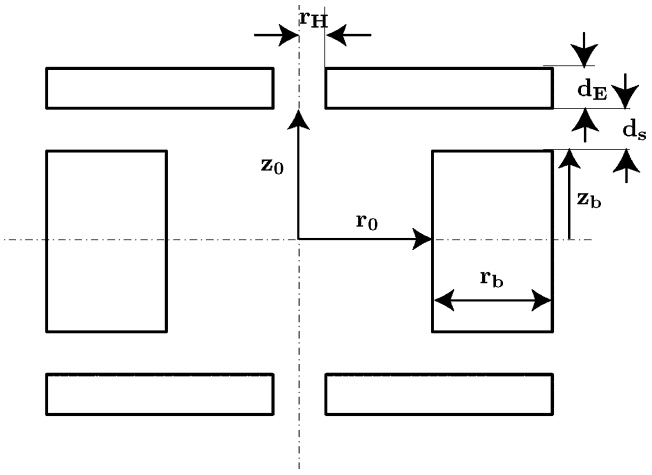

Fig. 4. Geometry of the cylindrical ion trap mass analyzer indicating the different geometry parameters.

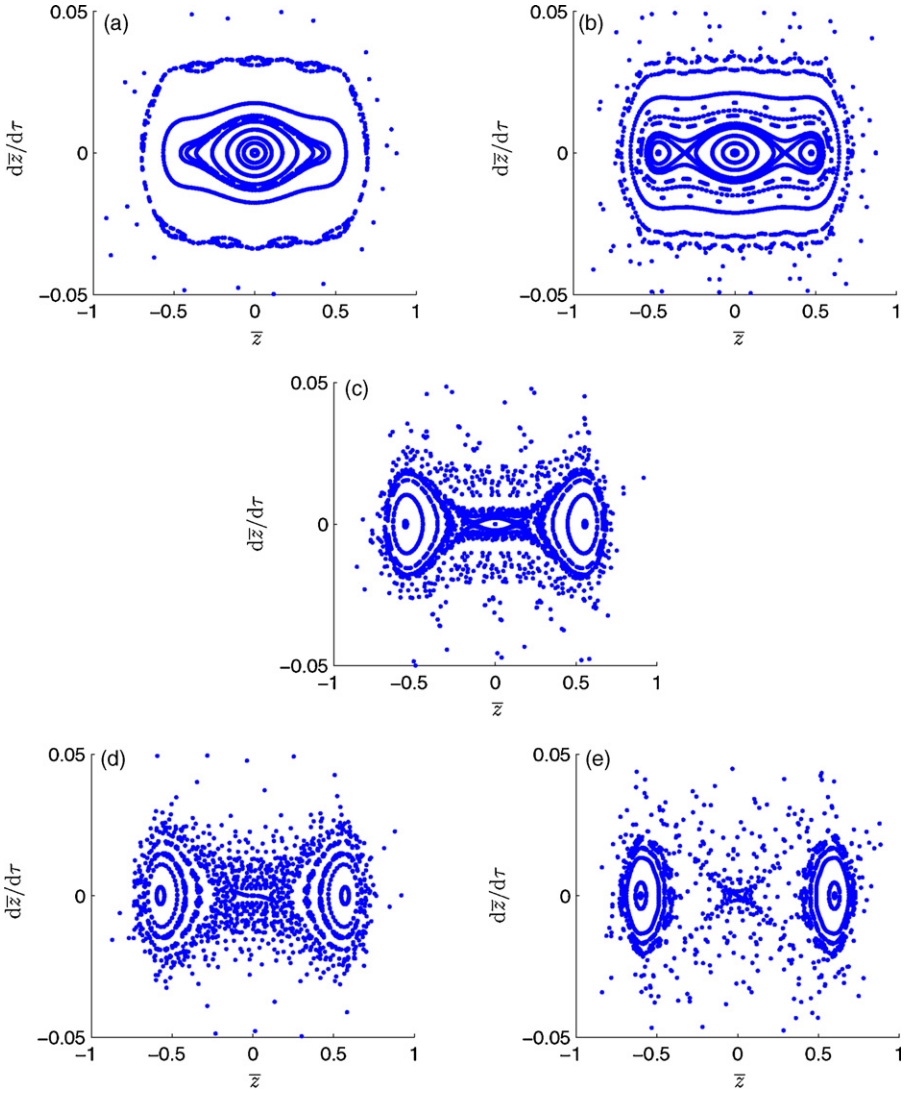

Fig. 5. Poincaré sections for the CIT0 for different values of q_z equal to (a) 0.898, (b) 0.9, (c) 0.906, (d) 0.908 and (e) 0.912.

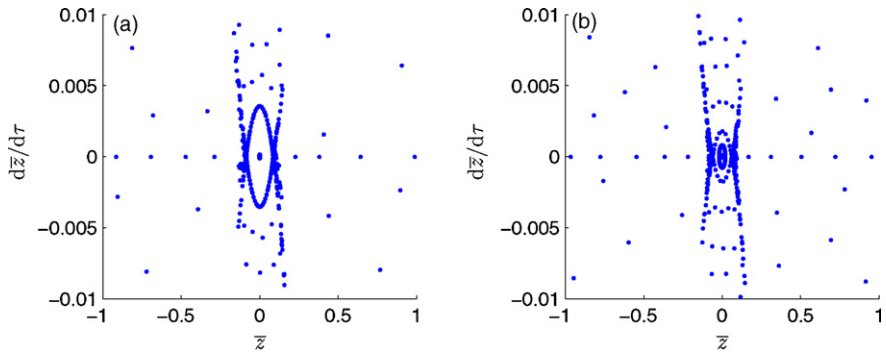

Fig. 6. Poincaré sections for the CITopt for different values of q_z (a) 0.896 and (b) 0.902.

and eventually only a saddle is left at the origin. However, we see that the stable centers away from the origin remain intact.

The reason for the relatively poor resolution associated with the CIT0 is the negative dodecapole ratio, A_6/A_2, which incidentally also has the largest magnitude among the first few higher order multipoles. The contribution of dodecapole superposition can be seen in the outlying centers in the Poincaré plots. The stable region close to the origin is on account of the presence of the positive even multipoles.

Recognizing that A_6/A_2 has to be positive for improving the resolution of the CIT0, we have optimized the CIT geometry with this restriction. We have carried out a one parameter optimization involving only z_b, half the cylinder length, and all the other parameters have been kept fixed to their values in the CIT0. This was done with a view of easy retrofitting of a cylinder with a new dimension on an existing mechanical assembly. The objective function, F_1, used for the optimization is

$$F_1 = \left| \frac{A_6}{A_2} - c_2 \right|, \quad c_2 = 0.002647.$$

F_1 ensures that A_6/A_2 is positive and has a value close to c_2, the value of A_6/A_2 in the stretched Paul trap. Starting with appropriate initial conditions, A_4/A_2 can also be ensured to be positive.

The optimized multipole coefficients are presented in Table 4 under the column CITopt. It can be seen that A_6/A_2 in the optimized geometry has a value of 0.002650, which is close to our desired value, although the value of A_4/A_2 is considerably higher at 0.961229, compared to 0.073958 in the CIT0. Also seen in the table are the ratios A_8/A_2, A_{10}/A_2 which are considerably higher than their values in the CIT0, with these ratios appearing with a negative sign. The value of F_1 at the optimum is 0.000003.

In order to check the ion dynamics within the CITopt, we plotted the Poincaré sections using Eq. (11) with the weights of multipole field reported in Table 4. Fig. 6 presents these Poincaré sections for q_z corresponding to 0.896 and 0.902, close to the stability boundary of the Mathieu stability plot. It is evident from these plots that the negative contribution of A_8/A_2 and A_{10}/A_2 is adequately compensated for by the strong influence of A_4/A_2 since the Poincaré sections reveal only one stable region close to the origin with no hint of outlying stable centers as was observed for the CIT0 in Fig. 5. Based on these observations, it appears that the performance of the CITopt may be better than that of the CIT0. Note, however, that A_4/A_2 is unusually large ($A_4/A_2 = 0.961$ when normalized with respect to z_0, and $A_4/A_2 = 0.398$ when normalized with respect to r_0) and such large numbers have not been reported for other mass analyzers in the mass spectrometry literature. Consequently, the CITopt will need to be further investigated before this geometry can be accepted (see also the concluding paragraphs of Section 4.4).

Table 5
Comparison of geometry parameters of the optimized geometry, the CITopt, with the CIT0

	r_0	z_0	z_b	d_s	r_b	d_E	r_h	z_0/r_0
CITopt	5.0	7.7743	6.1743	1.6	4.5	0.3	0.5	1.5549
CIT0	5.0	5.0	3.4	1.6	4.5	0.3	0.5	1.0

All the geometry parameters are as described in Ref. [1].

The geometry parameters for the CITopt is presented in Table 5, which also includes the parameters for the CIT0 reported in Ref. [1] for the purpose of comparison.

Our attempt to further optimize CIT with the restriction that both A_4/A_2 and A_6/A_2 should have values similar to the stretched geometry Paul trap did not yield useful results. Based on our understanding that this was due to having too few geometry parameters in the design, we took up for investigation two new geometries, one with a step at the center of the cylinder ring electrode and the other with a step on the endcap electrode. These new geometries give us the requisite degrees of freedom in the geometry to achieve field configurations similar to that in the stretched geometry Paul trap.

4.2. SRIT

Fig. 7 presents the geometry parameters of the stepped ring electrode ion trap (SRIT) that we have taken up for study. r_0 and r_1 correspond to the two radii associated with the cylinder; z_e and r_b correspond to the thicknesses of the endcap and ring electrodes, respectively; r_h is the radius of the hole at the center of the endcap electrodes; a, b and z_0 correspond to the half-height of the step, half-height of the cylinder, and the distance from the center of the trap to the endcap electrodes, respectively.

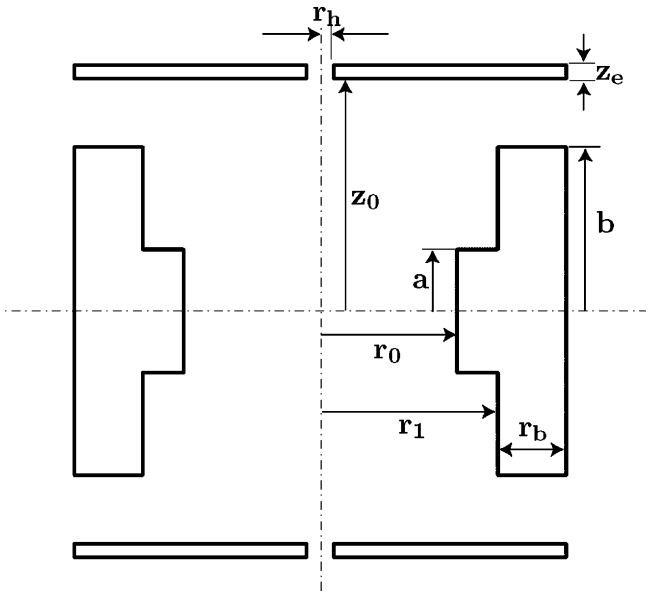

Fig. 7. Geometry of the stepped cylinder ion trap mass analyzer indicating the different geometrical parameters.

In our optimization process, the parameters r_h, r_b and z_e are kept constant because it was observed in our preliminary studies that the thickness of the electrodes (r_b, z_e) did not have a significant effect on the multipole coefficients. Further, the radius of the endcap holes (r_h) is held constant because we wish to optimize the geometry for a given hole size. With this, only r_1, a, b and z_0 are optimized in our present study. All the dimensions have been normalized with respect to r_0, the smaller radius associated with the cylinder.

4.2.1. SRIT1 and SRIT2

We have carried out the optimization using two separate objective functions, F_2 and F_3, which are

$$F_2 = \left|\frac{A_4}{A_2} - c_1\right| + \left|\frac{A_6}{A_2} - c_2\right|, \quad c_1 = 0.009880,$$

$$c_2 = 0.002647$$

and

$$F_3 = \left|\frac{A_4}{A_2} - c_1\right| + \left|\frac{A_6}{A_2} - c_2\right| + \left|\frac{A_8}{A_2} - c_3\right|, \quad c_1 = 0.009880,$$

$$c_2 = 0.002647, \quad c_3 = 0.000215$$

In the first objective function, F_2, two higher order multipoles, A_4 and A_6 (in addition to the quadrupole component A_2) have been used in the optimization while in the second, F_3, an additional multipole weight A_8 has been included in the optimization. The motivation was to explore the differences in the geometries recommended by these two objective functions.

We call the optimized geometry that is obtained using the objective function F_2 as the SRIT1 and that obtained using F_3 as the SRIT2. At the end of the optimization, the resulting geometry is expected to have A_4/A_2 and A_6/A_2 close to 0.009880 and 0.002647, respectively, for the SRIT1 and A_4/A_2, A_6/A_2 and A_8/A_2 to be close to 0.009880, 0.002647 and 0.000215, respectively, for the SRIT2. These multipole coefficients correspond to the respective values for the stretched geometry Paul trap seen in Table 4. The values of the multipole coefficients for the SRIT1 and the SRIT2, obtained consequent to our optimization, are presented in Table 4.

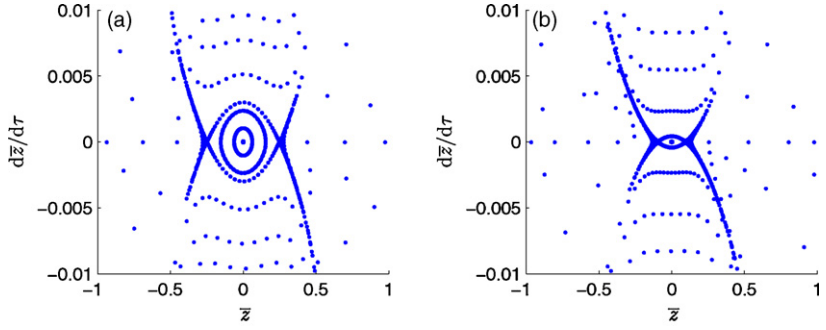

Fig. 8. Poincaré sections for the SRIT1 for q_z equal to (a) 0.907 and (b) 0.9079.

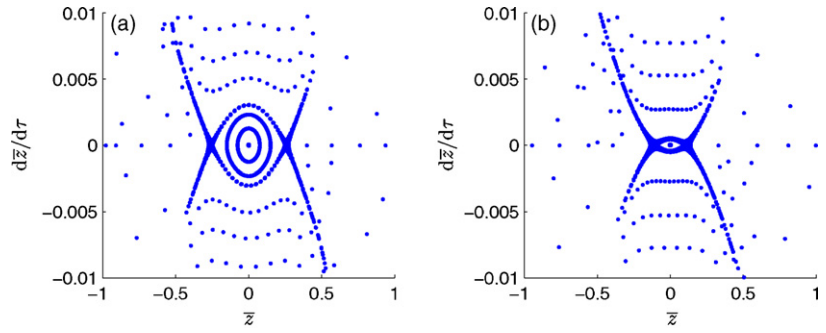

Fig. 9. Poincaré sections for the SRIT2 for q_z equal to (a) 0.907 and (b) 0.9079.

Table 6
Geometry parameters of the optimized geometries the SRIT1 and the SRIT2

	r_0	r_1	a	b	z_0	r_h	r_b	z_e	r_0/r_1	a/b
SRIT1	1.0	1.3966	0.2803	1.1445	1.6233	0.1	0.5	0.1	0.7160	0.2449
SRIT2	1.0	1.3919	0.2737	1.2144	1.5049	0.1	0.5	0.1	0.7184	0.2254

As expected, the SRIT1 forces A_4/A_2 and A_6/A_2 to the values close to those reported for the stretched Paul trap and the value of F_2 at the optimum is 0.000038. However, the weights of higher order multipoles are considerably larger and A_{10}/A_2 even has a negative sign. Poincaré sections for the SRIT1, presented in Fig. 8a and b for q_z values of 0.907 and 0.9079, respectively, however suggest that these higher order multipoles do not cause any deterioration in performance and that the deleterious effect of A_{10}/A_2 is compensated for by the other even multipoles.

The weights of the multipoles for the SRIT2 are also presented in Table 4 and the value of F_3 at the optimum is 0.000236. Here too, as desired, the ratios of A_4/A_2, A_6/A_2 and A_8/A_2 have been forced to the values close to that seen in the stretched geometry Paul trap. Further, A_{10}/A_2 and A_{12}/A_2 have lower weights compared to the SRIT1, although A_{10}/A_2 is still negative. The Poincaré sections for q_z values of 0.907 and 0.9079 shown in Fig. 9a and b, respectively, display a similar structure as in the SRIT1 and they suggest that the SRIT2 too will display good performance. We will investigate the coupled radial/axial dynamics of both the SRIT1 and the SRIT2 below.

The geometry parameters of the SRIT1 and the SRIT2 are presented in Table 6. As mentioned earlier, all the dimensions are normalized with respect to the parameter r_0 and the parameters that have been optimized are r_1, a, b and z_0. The parameters r_h, r_b and z_e have been fixed at the values shown in Table 6. Also included in the table are r_0/r_1 and a/b, which correspond to the ratio of the two radii associated with the cylinder and the ratio of half-height of the step to half-height of the cylinder. The aspect ratios (z_0/r_0) are 1.6233 and 1.5049 for the SRIT1 and the SRIT2, respectively.

In the SRIT1 and the SRIT2 the higher multipole weights, not being included in the objective functions, are large as seen in Table 4. Though the Poincaré sections (which include all even multipoles up to A_{12}) for the SRIT1 and the SRIT2 suggest good performance, it is interesting to seek a geometry where the growth in non-minimized multipole strengths is slower. Hence, we have investigated yet another trap geometry, in which there is a step in the endcap electrode instead of the central ring electrode, the SEIT.

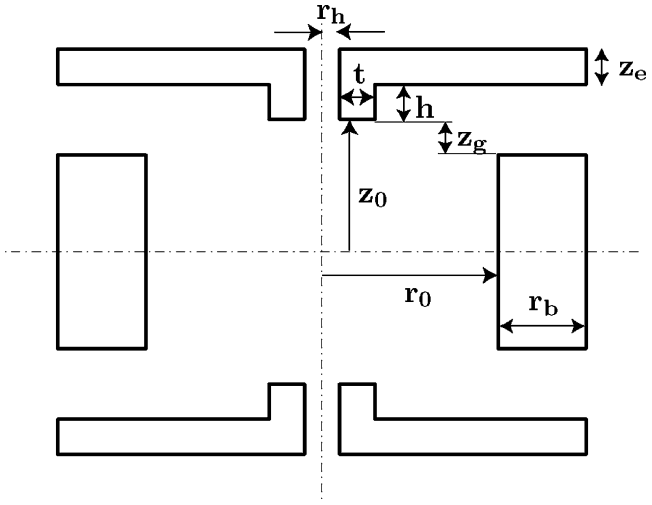

Fig. 10. Geometry of the stepped endcap cylindrical ion trap mass analyzer indicating the different geometry parameters.

4.3. SEIT

The SEIT geometry is presented in Fig. 10. As in the case of SRIT, the thicknesses of the endcap electrode (z_e) and the central ring electrode (r_b), as well as the endcap hole radius, r_h, have been held constant. Additionally, the gap between the central ring electrode and the endcap electrode, z_g, has also been kept constant. The parameters that have been optimized are z_0, t and h, which correspond to the distance of the endcap from the center of the trap, the thickness of the step and the height of the step, respectively. All dimensions of the geometry have been normalized with respect to the radius of the central ring electrode, r_0. In the SRIT1 and the SRIT2, we have seen that the coefficients not included in the objective functions are high and that A_{10}/A_2 is actually negative. Hence, in optimizing the

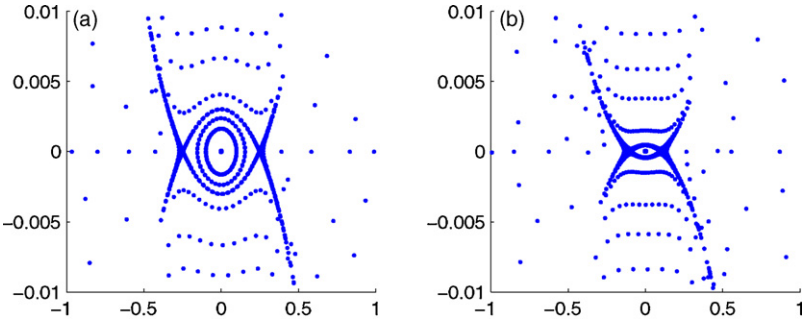

Fig. 11. Poincaré sections for the SEIT for q_z equal to (a) 0.907 and (b) 0.9079.

Table 7
Geometry parameters of the SEIT geometry

	r_0	z_0	t	h	r_h	r_b	z_e	z_g
SEIT	1.0	0.7392	0.0674	0.1176	0.1	0.5	0.2	0.2

SEIT geometry, we have attempted to get A_4/A_2 and A_6/A_2 to match the stretched Paul trap while keeping the higher coefficients small *and* positive. The objective function that has been used is

$$F_4 = \left|\frac{A_4}{A_2} - c_1\right| + \left|\frac{A_6}{A_2} - c_2\right| + \sum_{n=8}^{12}\left|\frac{A_n}{A_2}\right| - 100\sum_{n=8}^{12} H\left(-\frac{A_n}{A_2}\right)\frac{A_n}{A_2}$$

where $c_1 = 0.009880$, $c_2 = 0.002647$

and $H(x) = \begin{cases} 1 & \text{if } x \geq 0 \\ 0 & \text{if } x < 0. \end{cases}$

$H(x)$ in the above equation is the Heaviside function. The first two terms in F_4 are similar to the ones in the earlier objective functions. The third term is the sum of the absolute values of the ratios of the higher order multipole coefficients (A_8 to A_{12}) to A_2. This term ensures that the magnitudes of these ratios are small. The fourth term penalizes negative multipole coefficients. This term forces the optimization toward geometries for which there are no negative even multipoles or only a few with very small magnitudes. Note that F_4 can only be positive or zero.

The multipole coefficients for the SEIT are presented in Table 4. The ratios A_4/A_2 and A_6/A_2 match up to four and three decimal places, respectively, with those of the stretched Paul trap. A_8, A_{10} and A_{12} are smaller than those in the CITopt, the SRIT1 and the SRIT2 and more importantly, they are positive. On account of these features, the SEIT has a field distribution closest to the stretched geometry Paul trap. As expected, the Poincaré sections for the SEIT in Fig. 11a and b predict good performance.

The geometry parameters of the SEIT are presented in Table 7. As mentioned earlier, all the dimensions are normalized with respect to the parameter r_0 and the parameters that have been optimized are z_0, t and h. The parameters r_h, r_b, z_e and z_g have been fixed to the values shown in Table 7. The aspect ratio (z_0/r_0) is 0.7392.

4.4. Stability of radial motion

The focus so far has been on the axial motion of ions, because in conventional mass spectrometry experiments in rf ion traps, ion destabilization in the z direction is used to obtain the mass spectrum of the analyte compound. However, in the context of the newer traps under discussion in this paper, it is necessary to probe radial direction motion to ensure that coupling or other nonlinear effects do not destabilize the ion in the radial direction *prior* to their z direction instability.

The numerical simulations we present use the coupled nonlinear Mathieu equation for a single ion for $a_z = 0$. The equations of motion in the z and r directions (see Appendix A for details of the derivation) are respectively,

$$\frac{d^2\bar{z}}{d\tau^2} + \frac{2c}{\Omega}\frac{d\bar{z}}{d\tau} + 2q_z\cos 2\tau\sum_{n=1}^{6}\frac{A_{2n}}{2A_2} \times \left(2n\bar{\rho}^{2n-2}P_{2n}(\cos\theta)\bar{z} + \bar{\rho}^{2n-3}\frac{dP_{2n}(\cos\theta)}{d\cos\theta}\bar{r}^2\right) = 0 \quad (12)$$

and

$$\frac{d^2\bar{r}}{d\tau^2} + \frac{2c}{\Omega}\frac{d\bar{r}}{d\tau} + 2q_z\cos 2\tau\sum_{n=1}^{6}\frac{A_{2n}}{2A_2} \times \left(2n\bar{\rho}^{2n-2}P_{2n}(\cos\theta)\bar{r} - \bar{\rho}^{2n-3}\frac{dP_{2n}(\cos\theta)}{d\cos\theta}\bar{r}\bar{z}\right) = 0, \quad (13)$$

where $\cos\theta = \bar{z}/\bar{\rho}$, $\bar{z} = z/L_N$ is the normalized axial position of the ion (L_N is the normalizing length), $\bar{r} = r/L_N$ the normalized radial position of the ion, $\bar{\rho} = \sqrt{\bar{z}^2 + \bar{r}^2}$, P_n the nth Legendre polynomial, $\tau = \Omega t/2$, Ω the angular frequency of the applied rf potential, c the damping coefficient, and q_z is the Mathieu parameter given by

$$q_z = \frac{4qA_2V}{mL_N^2\Omega^2}, \quad (14)$$

where in turn q/m is the charge to mass ratio of the ion, V the zero-to-peak amplitude of the applied rf potential and L_N is chosen here as half the distance between the endcap electrodes. Note that it is more common in the literature to use a symbol $q_r = -q_z/2$ for the radial motion equation. However, here the use of q_z in the radial equation is correct because the appropriate (θ-dependent) potential has been used. In Eqs. (12) and (13) we have used the viscous drag model of damping proposed by Goeringer et al. [34],

$$c = \frac{m_n}{m+m_n}\frac{p}{kT_b}\frac{q}{2\epsilon_0}\sqrt{\alpha\frac{m+m_n}{mm_n}}, \quad (15)$$

where m_n is the mass of the bath gas (helium), $\alpha = 0.22 \times 10^{-40}\,\mathrm{F\,m^2}$ the polarizability of the bath gas, $\epsilon_0 = 8.854 \times 10^{-12}\,\mathrm{F/m}$ the permittivity of free space, T_b the temperature (chosen to be 298 K), p the pressure of the bath gas, k the Boltzmann constant and m is the mass of the ion.

Simulations have been done using MATLAB to follow the evolution of axial and radial motion of an ion of mass 78 Th. Starting from $q_z = 0.6$ (for ions of 78 Th) q_z is increased linearly with time until the ion becomes unstable. The scan used is

$$\frac{dq_z}{d\tau} = 2.058 \times 10^{-5}. \quad (16)$$

This corresponds to a scan rate of approximately 180 μs/Th.

In the simulations helium bath gas pressure of 0.1 Pascal has been used, and the rf frequency has been taken to be 1 MHz ($\Omega = 2\pi \times 10^6$). In all the simulations, q_z starts at 0.6 and is varied as per Eq. (16) until the ion becomes unstable.

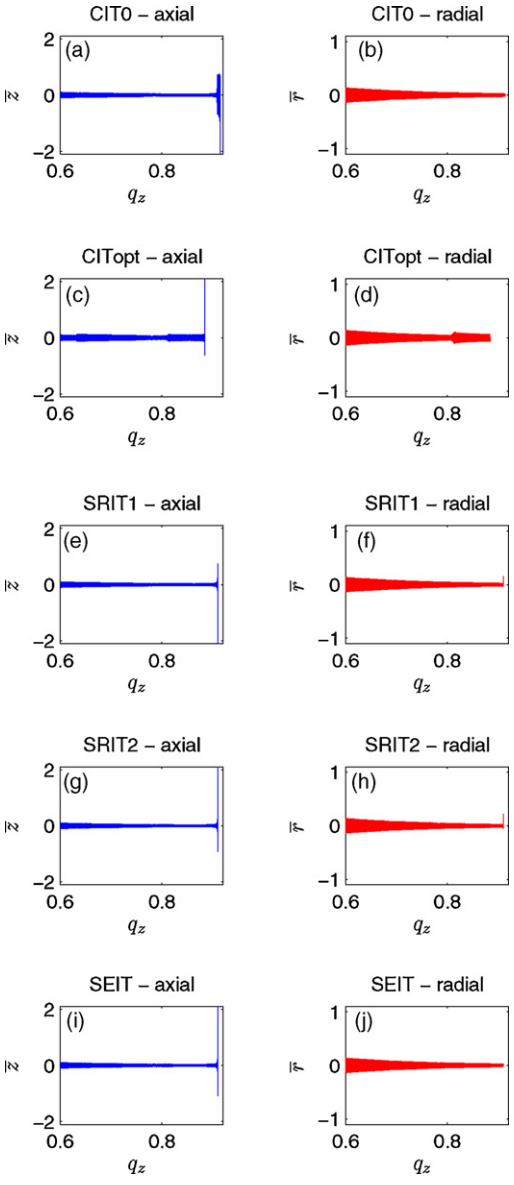

Fig. 12. (a), (c), (e), (g) and (i) show $\bar{z}$ trajectories with q_z for the CIT0, the CITopt, the SRIT1, the SRIT2 and the SEIT, respectively. (b), (d), (f), (h) and (j) show $\bar{r}$ trajectories with q_z for the CIT0, the CITopt, the SRIT1, the SRIT2 and the SEIT, respectively.

Fig. 12 shows the time trajectories of $\bar{z}$ and $\bar{r}$ for the traps considered in this paper. Fig. 12a, c, e, g and i shows $\bar{z}$ trajectories with scaled time τ for the CIT0, the CITopt, the SRIT1, the SRIT2 and the SEIT, respectively. Fig. 12b, d, f, h and j shows $\bar{r}$ trajectories with scaled time τ for the CIT0, the CITopt, the SRIT1, the SRIT2 and the SEIT, respectively. The initial conditions of the ions for all the traps are

$$\bar{z}(0) = 0.1, \quad \frac{d\bar{z}}{d\tau}(0) = 0, \quad \bar{r}(0) = 0.1, \quad \frac{d\bar{r}}{d\tau}(0) = 0.$$

It can be seen from Fig. 12 that the ion motion in all the cases is stable in the radial direction and instability only sets in near the nominal stability boundary.

We mention that, in other simulations, setting $\bar{z} = \bar{r} = 0.2$ led to premature growth in axial and radial motion for the CITopt.

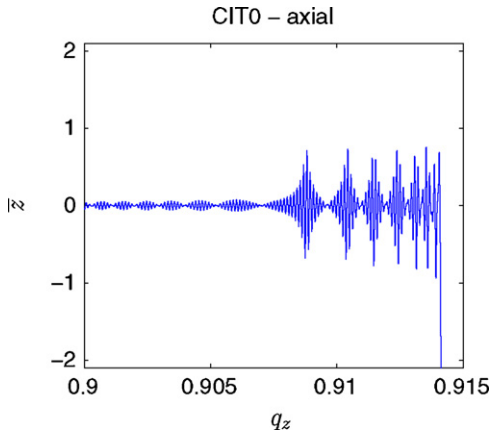

Fig. 13. Axial motion of an ion in CIT0 prior to ejection. Zoomed portion of the plot in Fig. 12a.

Further, even setting $\bar{z} = \bar{r} = 0.4$ for the SEIT gave appropriately bounded axial motions right up to the nominal stability boundary, reinforcing our view that the SEIT is most likely to give superior performance among the geometries considered in this paper.

Finally, in contrast to the SEIT, we now examine the cylindrical geometries (the CIT0 and the CITopt) further. The two visible jumps in amplitude in Fig. 12c with one corresponding jump visible in Fig. 12d, are most likely due to passage through internal nonlinear resonances. Note that the CITopt is the most strongly nonlinear trap among those studied here.

A zoomed portion of Fig. 12a is shown in Fig. 13, where it is seen that, just prior to ejection, the ion has rapidly modulated oscillations of amplitude comparable to the trap dimension. Such dynamics, which is missing in the trap geometries proposed in this paper, may be compromising the performance in the CIT0.

4.5. Design sensitivity

We have studied the design sensitivity of one of the SRIT's (SRIT1) and the SEIT by varying each parameter by 0.01 units of nondimensionalized length from their optimum values. Table 8 shows the changes in the coefficients A_2, A_4 and A_6 for the SRIT1. Also shown are the resultant changes in the ratios A_4/A_2 and A_6/A_2. Table 9 shows the relative changes (percentage) in these coefficients for the SRIT1.

It is seen from Tables 8 and 9, that the coefficients do not change appreciably from their values at the optimum geometry, except perhaps with changes in a (step height). Thus if SRIT's are fabricated for experimental test-

Table 8
Changes in the coefficients with a variation of 0.01 units in the parameters (r_1, a, b, c) from their optimized values in the SRIT1

	ΔA_2	ΔA_4	ΔA_6	$\Delta(A_4/A_2)$	$\Delta(A_6/A_2)$
r_1	−0.00520	0.01272	−0.00503	−0.01434	0.00564
a	−0.00051	−0.00666	0.02758	0.00751	−0.03114
b	0.00279	−0.00435	−0.00140	0.00496	0.00160
z_0	−0.00072	−0.00178	−0.00154	0.00201	0.00173

Table 9
Relative changes (percentage) in the coefficients with an increase of 0.01 units in the parameters (r_1, a, b, c) from their optimized values in the SRIT1

	$\%A_2$	$\%A_4$	$\%A_6$	$\%(A_4/A_2)$	$\%(A_6/A_2)$
r_1	0.587	−145.367	212.118	−145.102	210.295
a	0.058	76.122	−1162.011	76.020	−1161.400
b	−0.315	49.731	59.100	50.205	59.602
z_0	0.081	20.402	64.775	20.304	64.641

Table 10
Changes in the coefficients with a variation of 0.01 units in the parameters (z_0, t, h) from their optimized values in the SEIT

	ΔA_2	ΔA_4	ΔA_6	$\Delta(A_4/A_2)$	$\Delta(A_6/A_2)$
z_0	−0.00686	−0.00262	0.00210	0.00479	−0.00398
t	−0.00220	−0.00164	−0.00053	0.00305	0.00099
h	0.00317	−0.00486	−0.00276	0.00935	0.00529

Table 11
Relative change (percentage) in the coefficients with an increase of 0.01 units in the parameters (z_0, t, h) from their optimized values in the SEIT

	$\%A_2$	$\%A_4$	$\%A_6$	$\%(A_4/A_2)$	$\%(A_6/A_2)$
z_0	1.303	50.943	−168.891	49.001	−168.005
t	0.417	31.760	42.376	31.213	41.784
h	−0.602	94.376	221.200	95.553	223.145

ing, the step height must be machined to higher dimensional accuracy.

Table 10 presents corresponding results for the SEIT. Table 11 shows the relative changes. Both the designs, the SRIT1 and the SEIT, look reasonable, though the SEIT seems better.

5. Conclusions

In this paper we have presented optimization of geometries of axially symmetric rf ion traps for mass analyzers. The Nelder-Mead simplex method was used to obtain the geometry parameters of the mass analyzers by using objective functions which incorporate desired weights of multipole field coefficients. Multipole coefficients up to A_{12} have been considered in our optimization of the CITopt, the SRIT1, the SRIT2 and the SEIT. Poincaré sections, obtained by numerically integrating the nonlinear Mathieu equation, have been used to evaluate trap performance.

A departure that we have made in this paper from conventional usage is in regard to our choice of the scaling length, L_N. In our study, we have chosen z_0 to be the scaling length and we recomputed multipole coefficients of the stretched geometry Paul trap for the purpose of comparison as well as for its adaptation to the cylindrical geometries. This choice has been motivated by our primary interest in the z-direction motion.

With a view towards future experimental implementations, we draw the reader's attention afresh to Eqs. (8) and (10). The computation of A_2 (see Eq. (8)) implicitly includes the normalizing length L_N. Subsequently, the voltage V at the nominal stability boundary of $q_z = 0.908$ (see Eq. (10)) depends on both A_2 (as reported in our tables) and L_N (used here as half the distance between the endcaps).

An important question that we have only partially addressed in this paper is what multipole composition might lead to good traps. Here, we have assumed that even multipole superpositions that are both small and positive are desirable. Beyond this criterion and our numerical simulation, however, it seems that there is an important role to be played by multi-particle simulation packages such as ITSIM [12], AXSIM [35] and SIMION [36].

Acknowledgment

We would like to thank two anonymous reviewers for their comments. Section 4.4 is a result of the caution expressed by one of them.

Appendix A. Derivation of equations of motion

Starting with the expression for the potential in Eq. (4), we derive the equation of motion in the z direction. The equation for r direction motion can be similarly derived.

The potential at a point $u(\rho, \theta, \phi)$ in spherical coordinates, in an axially symmetric trap, can be expressed in terms of Legendre polynomials P_n. When a potential Φ is applied to the central electrode with endcaps kept at ground potential, $u(\rho, \theta, \Phi)$ is given by [28]

$$u(\rho, \theta, \phi) = \Phi \sum_{n=0}^{\infty} A_n \left(\frac{\rho}{L_N}\right)^n P_n(\cos\theta) \tag{A.1}$$

where A_n are the multipole coefficients and L_N is a normalizing length.

The z component of the electric field, E_z, is $-\partial u/\partial z$. Hence, differentiating Eq. (A.1) with respect to z; and considering only the even order terms (assuming top-bottom symmetry of the trap, as has been assumed in this paper) we have:

$$-E_z = \frac{\partial u}{\partial z} = \Phi \sum_{n=0}^{\infty} A_{2n} \left(\frac{1}{L_N}\right)^{2n} \times \left(\frac{\partial \rho^{2n}}{\partial z} P_{2n}(\cos\theta) + \rho^{2n} P'_{2n}(\cos\theta) \frac{\partial \cos\theta}{\partial z}\right) \tag{A.2}$$

where $P'_{2n}(\cos\theta)$ is the derivative of $P_{2n}(\cos\theta)$ with respect to $\cos\theta$. Noting that $\cos\theta = z/\sqrt{z^2 + r^2}$ and $\rho = \sqrt{z^2 + r^2}$, we get:

$$-E_z = \frac{\partial u}{\partial z} = \Phi \sum_{n=0}^{\infty} A_{2n} \left(\frac{1}{L_N}\right)^{2n} \times \left(2n\rho^{2n-2} P_{2n}(\cos\theta) z + \rho^{2n-3} P'_{2n}(\cos\theta) r^2\right). \tag{A.3}$$

Using

$$m \frac{\mathrm{d}^2 z}{\mathrm{d}t^2} = E_z q, \tag{A.4}$$

we obtain

$$m\frac{d^2z}{dt^2} = -\Phi\sum_{n=0}^{\infty}A_{2n}\left(\frac{1}{L_N}\right)^{2n} \times \left(2n\rho^{2n-2}P_{2n}(\cos\theta)z + \rho^{2n-3}P'_{2n}(\cos\theta)r^2\right)q. \quad (A.5)$$

We now make the substitutions $\Phi = U + V\cos(\Omega t)$, $t = 2\tau/\Omega$ and $z = L_N\bar{z}$, where U is the dc potential applied to the ring electrode, V the amplitude of the rf potential, Ω the frequency of the rf potential, τ the scaled time and $\bar{z}$ is the normalized axial position of the ion. Rearranging the terms, we obtain

$$\frac{d^2\bar{z}}{d\tau^2} + (a_z + 2q_z\cos 2\tau)\sum_{n=1}^{\infty}\frac{A_{2n}}{2A_2} \times \left(2n\bar{\rho}^{2n-2}P_{2n}(\cos\theta)\bar{z} + \bar{\rho}^{2n-3}\frac{dP_{2n}(\cos\theta)}{d\cos\theta}\bar{r}^2\right) = 0, \quad (A.6)$$

where a_z and q_z are given by

$$a_z = \frac{8qA_2U}{mL_N^2\Omega^2}, \qquad q_z = \frac{4qA_2V}{mL_N^2\Omega^2}.$$

This is the coupled nonlinear Mathieu equation for a single ion in the axial direction in its general form. In mass selective boundary ejection experiments the dc potential, U, is usually set to zero which causes a_z, in Eq. (A.6), to vanish. Introducing a viscous damping term in Eq. (A.6), noting the stretched time scale in the equation and truncating to $n = 6$, we get Eq. (12) used in Section 4.4.

Eq. (13) used in Section 4.4 can be similarly derived.

References

[1] G. Wu, R.G. Cooks, Z. Ouyang, Int. J. Mass Spectrom. 241 (2005) 119.
[2] D.B. Langmuir, R.V. Langmuir, H. Shelton, R.F. Wuerker, Containment Device, U.S. Patent 3,065,640 (1962).
[3] M.N. Benilan, C. Audoin, Int. J. Mass Spectrom. Ion Phys. 11 (1973) 421.
[4] R.F. Bonner, J.E. Fulford, R.E. March, G.F. Hamilton, Int. J. Mass Spectrom. Ion Phys. 24 (1977) 255.
[5] R.E. Mather, R.M. Waldren, J.F.J. Todd, R.E. March, Int. J. Mass Spectrom. Ion Phys. 33 (1980) 201.
[6] J.M. Wells, E.R. Badman, R.G. Cooks, Anal. Chem. 70 (1998) 438.
[7] E.R. Badman, R.C. Johnson, W.R. Plass, R.G. Cooks, Anal. Chem. 70 (1998) 4896.
[8] Z. Ouyang, E.R. Badman, R.G. Cooks, Rapid Commun. Mass Spectrom. 13 (1999) 2444.
[9] G.E. Patterson, A.J. Guymon, L.S. Riter, M. Everly, J. Griep-Raming, B.C. Laughlin, Z. Ouyang, R.G. Cooks, Anal. Chem. 74 (2002) 6145.
[10] A.M. Tabert, J. Griep-Raming, A.J. Guymon, R.G. Cooks, Anal. Chem. 75 (2003) 5656.
[11] J.E.P. Syka, In: R.E. March, J.F.J. Todd (Eds.), Practical Aspects of Ion Trap Mass Spectrometry, vol. I, CRC Press, New York, pp. 169–205, 1995.
[12] H.A. Bui, R.G. Cooks, J. Mass Spectrom. 33 (1998) 297.
[13] J. Franzen, Int. J. Mass Spectrom. Ion Process. 125 (1993) 165.
[14] J. Franzen, Int. J. Mass Spectrom. Ion Process. 130 (1994) 15.
[15] Y. Wang, J. Franzen, K.P. Wanczek, Int. J. Mass Spectrom. Process. 124 (1993) 125.
[16] Y. Wang, J. Franzen, Int. J. Mass Spectrom. Ion Process. 132 (1994) 155.
[17] M. Sudakov, Int. J. Mass Spectrom. 206 (2001) 27.
[18] R.E. Kaiser, J.N. Louris, J.W. Amy, R.G. Cooks, Rapid Comm. Mass Spectrom. 3 (1989) 225.
[19] J.D. Williams, K.A. Cox, R.G. Cooks, S.A. McLuckey, K.J. Hart, D.E. Goeringer, Anal. Chem. 66 (1994) 725.
[20] A. Makarov, Anal. Chem. 68 (1996) 4257.
[21] N. Rajanbabu, A. Chatterjee, A.G. Menon, Int. J. Mass Spectrom. 261 (2007) 159.
[22] N. Rajanbabu, A. Marathe, A. Chatterjee, A.G. Menon, Int. J. Mass Spectrom. 261 (2007) 170.
[23] G.T. Abraham, A. Chatterjee, A.G. Menon, Int. J. Mass Spectrom. 231 (2004) 1.
[24] W.R. Plass, H. Li, R.G. Cooks, Int. J. Mass Spectrom. 228 (2003) 237.
[25] C.N. Klahr, Operat. Res. 6 (1958) 849.
[26] E. Weber, Electromagnetic Fields: Theory and Applications, vol. I, Mapping Fields, John Wiley & Sons, New York, 1950.
[27] M. Abramowitz, I.A. Stegun, Handbook of Mathematical Functions, Dover Publications Inc., New York, 1970.
[28] E.C. Beaty, Phys. Rev. A 33 (1986) 3645.
[29] A. Chaudhary, F.H.W. van Ameroma, R.T. Short, S. Bhansali, Int. J. Mass Spectrom. 251 (2006) 32.
[30] J.A. Nelder, R. Mead, Comput. J. 7 (1965) 308.
[31] W.H. Press, S.A. Teukolsky, W.T. Vetterling, B.P. Flannery, Numerical Recipes in C, Cambridge University Press, Cambridge, 1992.
[32] O. Kornienko, P.T.A. Reilly, W.B. Whitten, J.M. Ramsey, Rapid Commun. Mass Spectrom. 13 (1999) 50.
[33] J. Franzen, R.-H. Gabling, M. Shubert, Y. Wang, In: R.E. March, J.F.J. Todd (Eds.), Practical Aspects of Ion Trap Mass Spectrometry, vol. I, CRC Press, New York, 1995, p. 69 (Chapter 3).
[34] D.E. Goeringer, W.B. Whitten, J.M. Ramsey, S.A. McLuckey, G.L. Glish, Anal. Chem. 64 (1992) 1434.
[35] M. Sudakov, S. Kumashiro, Simulations of High Resolution Resonance Ejection Scan in a Digital Ion Trap, Desorption 2004, St. Petersburg, Russia, August 28–September 2, 2004.
[36] D.A. Dahl, Int. J. Mass Spectrom. 200 (2000) 3.